2024 IEEE International Conference on Robotics and Automation (ICRA 2024)
May 13-17, 2024. Yokohama, Japan

Saturation-Aware Angular Velocity Estimation: Extending the Robustness of SLAM to Aggressive Motions*

Simon-Pierre Deschênes[1], Dominic Baril[1], Matěj Boxan[1],
Johann Laconte[1], Philippe Giguère[1] and François Pomerleau[1]

***Abstract*— We propose a novel angular velocity estimation method to increase the robustness of Simultaneous Localization And Mapping (SLAM) algorithms against gyroscope saturations induced by aggressive motions. Field robotics expose robots to various hazards, including steep terrains, landslides, and staircases, where substantial accelerations and angular velocities can occur if the robot loses stability and tumbles. These extreme motions can saturate sensor measurements, especially gyroscopes, which are the first sensors to become inoperative. While the structural integrity of the robot is at risk, the robustness of the SLAM framework is oftentimes given little consideration. Consequently, even if the robot is physically capable of continuing the mission, its operation will be compromised due to a corrupted representation of the world. Regarding this problem, we propose a method to estimate the angular velocity using accelerometers during extreme rotations caused by tumbling. We show that our method reduces the median localization error by 71.5 % in translation and 65.5 % in rotation and is robust to mapping failures, which occurred in 37.5 % of the experiments without our method. We also propose the Tumbling-Induced Gyroscope Saturation (TIGS) dataset, which consists of outdoor experiments recording the motion of a mechanical lidar subject to angular velocities four times higher than other similar datasets available. The dataset is available online at https://github.com/norlab-ulaval/Norlab_wiki/wiki/TIGS-Dataset.**

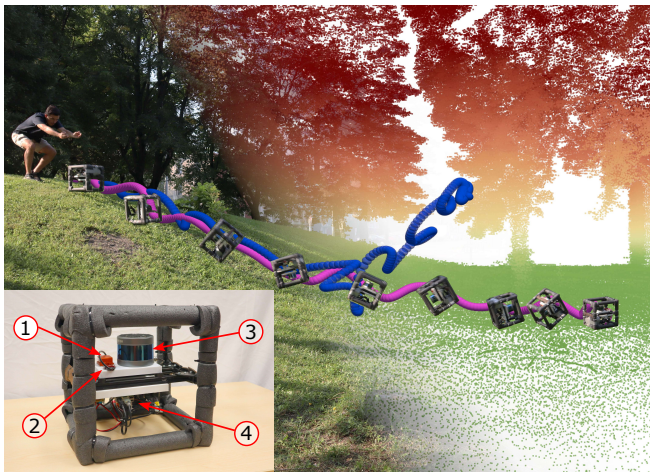

Fig. 1. Our robot localization system tumbling down a steep hill. At the top is a picture of the event and the reconstructed point cloud. The blue trajectory represents a SLAM-estimated trajectory relying on raw gyroscope measurements. In pink is a similar trajectory, which is estimated relying on our angular velocity estimation approach. The rugged perception rig is shown in the bottom left. The numbers in the red circles correspond to (1) XSens MTi-30 IMU, (2) VectorNav VN-100 IMU, (3) RoboSense RS-16 lidar, and (4) Raspberry Pi 4.

I. INTRODUCTION

For many robot applications, operations are conducted in a remote, or dangerous environment, where human intervention is impossible [1]. Hardware improvements have significantly reduced potential failure due to collisions, especially for aerial systems [2]. However, software systems, particularly robot localization, will typically not recover from falls, drops, and collisions [3]. Therefore, increasing mobile robot localization robustness to such events is key to enabling autonomy in human-denied environments. Inspired by work on control, such as Williams *et al.* [4], we define aggressive motions for perception as being near the dynamic limits that the system can sustain. With this definition, navigation on highways would not cause aggressive motions despite high velocities. On the contrary, a robot tumbling down a steep hill, as shown in the top part of Figure 1, exemplifies this definition of aggressive motions very well because of the repeated collisions and fast angular velocities that are sustained. Such motions cause skew in lidar scans [5] and saturation in gyroscope measurements [6]. Deskewing algorithms correct these distortions using an estimate of the intra-scan lidar motion. However, in many Simultaneous Localization And Mapping (SLAM) systems, the prior attitude for optimization and estimate for intra-scan lidar motion is obtained by integrating Inertial Measurement Unit (IMU) measurements [7]–[10]. Therefore, gyroscope saturations lead to wrong optimization priors, inaccurate deskewing, and thus, to SLAM failure, as shown by the blue trajectory. In this work, we propose to leverage the theory related to Gyro-free (GF) Inertial Navigation System (INS) [11] to estimate angular velocities during gyroscope saturations. To validate our approach without damaging robots, we built a rugged lidar-inertial rig, shown in the bottom left. We generated a dataset of the rig tumbling down a steep hill, saturating gyroscope measurements to analyze our solution. Thus, the contributions of this work are:

1) a novel method to estimate robot angular velocities during gyroscope saturation periods;
2) the Tumbling-Induced Gyroscope Saturation (TIGS) dataset, consisting of 32 distinct runs of a custom per-

*This research was supported by the Fonds de recherche du Québec – Nature et technologies (FRQNT) and by the Natural Sciences and Engineering Research Council of Canada (NSERC) through grant CRDPJ 527642-18 SNOW (Self-driving Navigation Optimized for Winter). The authors wish to thank Benoît Audet for his help with the experimental setup.

[1]Northern Robotics Laboratory, Université Laval, Quebec City, Quebec, Canada {simon-pierre.deschenes, francois.pomerleau}@norlab.ulaval.ca

ception rig tumbling down a steep hill, reaching angular velocities up to $18.6\,\mathrm{rad/s}$.

II. RELATED WORK

In this section, we describe recent work in the literature focused on localization and mapping under aggressive motions. In particular, we explain how these approaches were not tested or would not function in cases where gyroscope saturations occur during aggressive motions. Then, we describe existing GF-INS methods, aiming to estimate the angular velocity of a robot when gyroscope measurements are saturated. Lastly, we analyze mechanical lidar SLAM datasets and demonstrate that they are not suited to test our angular velocity estimation method.

1) SLAM robust to aggressive motions: Several SLAM algorithms were proposed to overcome the challenges posed by aggressive motions. In the FAST-LIO2 SLAM algorithm [9], an Iterated Extended Kalman Filter (IEKF) back-propagates the estimated state to deskew the point cloud after the prediction step. FAST-LIO2 was tested at angular speeds up to $21.7\,\mathrm{rad/s}$, without specifying accelerations and with no mention of gyroscope saturations. Another algorithm robust to aggressive motions is the DLIO SLAM algorithm [10]. In DLIO, scans are deskewed using the lidar motion estimated by integrating IMU measurements with a constant jerk and angular acceleration model. After roughly aligning the scan with the map through deskewing, the scan alignment is refined using the Generalized Iterative Closest Point (GICP) [12] registration algorithm. Their method was tested at angular velocities up to $3.6\,\mathrm{rad/s}$ and linear accelerations up to $19.6\,\mathrm{m/s^2}$, but was not tested under saturated gyroscope measurements. Although promising, the aforementioned methods use IMU measurements to compute the prior for their optimization process. If IMU measurements are incomplete because of saturations, they might lead the optimization to converge far from the true solution. An approach to tackle sensor failures is introduced in the LOCUS SLAM algorithm [13]. They introduce a health-monitoring module in their method to detect sensor malfunctions. In contrast, we propose an approach that not only detects but also recovers from gyroscope failures, as robots do not have a direct alternative for such measurements. To our knowledge, the only lidar-inertial SLAM framework which is robust to IMU saturations is Point-LIO [14]. It consists of an on-manifold Extended Kalman Filter (EKF) that registers each individual point to the closest plane as it is measured and that uses a kinematic model to model IMU measurements as an output. Point-LIO therefore does not need to deskew incoming scans and is more robust to IMU saturations. To test their method, the authors conducted experiments in which gyroscope saturations were encountered over smooth motions. In our previous work [5], we introduced a SLAM algorithm that takes into account the skewing uncertainty during registration. This allowed our localization and mapping algorithm to give more importance to certain portions of a scan that were less affected by scan skewing. However, since our method was not robust to gyroscope saturation, we limited our experiments to angular speeds up to $11\,\mathrm{rad/s}$ and linear accelerations up to $200\,\mathrm{m/s^2}$. The aforementioned limitations motivate the need for an angular velocity estimation method relying on other sensory measurements, which can be relied upon in the case of gyroscope saturations during aggressive motions.

2) Angular Velocity Estimation: Several solutions have been proposed to estimate gyroscope measurements during saturation periods. In the work of Dang *et al.* [15], the authors propose a smoothing algorithm to estimate saturated gyroscope measurements. They use an optimization algorithm based on the presence of zero-velocity intervals for motion tracking. Their method is well-suited in situations in which short gyroscope-saturated time windows occur during a continuous motion contained between zero-velocity periods. However, their method was not designed for cases where repeated collisions are sustained (e.g., when tumbling). Alternatively, Tan *et al.* [16] introduce an EKF exploiting the sinusoidal structure of magnetometer measurements to estimate the angular velocity of a monocopter, despite gyroscope saturations. In a situation where repeated collisions are sustained, a sinusoidal structure in magnetometer measurements cannot be assumed. Moreover, in robotics, magnetometers are often disregarded as their measurements are biased by proximal magnetic sources [17]. Another approach is explored in the work of Pachter *et al.* [11], where GF INS theory is applied to allow the estimation of the position, orientation, linear velocity, and angular velocity of an object in 3D using only accelerometers. Following this work, Lee *et al.* [6] proposed an EKF to estimate the angular velocity of a rotating plate using three accelerometers, which they validated experimentally. This solution was developed for aerospace applications and was not tested inside a SLAM framework. Since accelerometer-based methods have more potential than other work presented previously, we will build on these solutions to improve the robustness of SLAM algorithms under saturated gyroscope measurements.

3) Aggressive Motion Datasets: In order to demonstrate the improvement of SLAM reached through our speed estimation method, a dataset with aggressive motions and gyroscope saturations is required. We studied the mechanical lidar SLAM datasets that are most commonly used and that contain the most aggressive motions, namely the Newer College [18] and Hilti-Oxford [19] datasets. Because of its importance in the literature, we also studied the KITTI dataset [20]. The maximum angular velocity in all of these datasets combined is $4.7\,\mathrm{rad/s}$ and the maximum linear acceleration in all datasets combined is $30.7\,\mathrm{m/s^2}$. Since the motions in these datasets are not aggressive enough to cause gyroscope saturations, we propose the Tumbling-Induced Gyroscope Saturation (TIGS) dataset, which consists of a perception rig tumbling down a hill, with angular velocities up to $18.6\,\mathrm{rad/s}$ and linear accelerations up to $157.8\,\mathrm{m/s^2}$.

III. THEORY

To increase the robustness of SLAM algorithms to a robot tumbling or colliding with its environment, we develop a method that allows the estimation of the angular velocity of

a robot when its gyroscope measurements are saturated. The only prerequisite of our angular velocity estimation method is an estimate of the robot's Center Of Mass (COM) location. We provide the uncertainty of the estimated velocity to allow its use in probabilistic frameworks (e.g., Bayesian filtering). We then describe the SLAM framework in which our method is inserted. Our angular velocity estimation method implementation is freely available online to facilitate replicability.[1]

A. Angular Velocity Estimation

Inertial measurements during an event of a robot tumbling down a hill are shown in Figure 2. Gyroscope saturations usually occur during the middle section of the tumbling, when the angular velocities are at their highest. Accelerometers, on the other hand, tend to saturate less and, even if they do saturate, it is for a short period (e.g., during a collision), as opposed to gyroscopes, which can saturate for several seconds. We therefore have two distinct cases during which to estimate saturated gyroscope measurements: *i)* during free-fall and *ii)* during collisions. Indeed, the plateaus in the angular speed curve correspond to free-fall periods whereas the fast changes correspond to collisions, as indicated by the spikes in the acceleration curve.

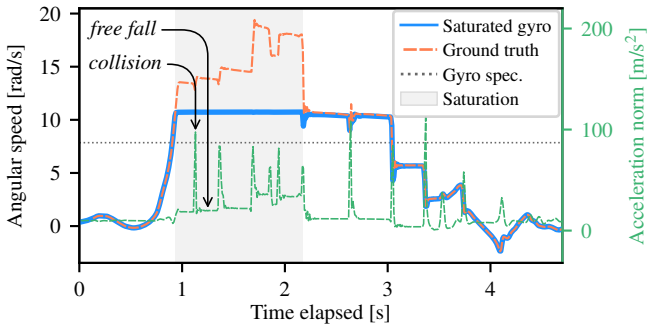

Fig. 2. The angular speed is shown through time for the saturated gyroscope axis of a robot tumbling down a hill. Light gray zones indicate the gyroscope saturation periods. The measurements from a saturated gyroscope are shown in blue, the ground-truth angular speeds are indicated in orange, and the norm of the measured acceleration is indicated in dashed green. We show the manufacturer-specified gyroscope saturation point in dark gray. Examples of collisions with the ground and free-fall events are highlighted.

Since the modeling of collisions is still an open problem, it is challenging to estimate the angular velocity from accelerometer measurements during collisions. Therefore, our approach is split into two steps. First, we estimate the angular velocities assuming free-fall conditions. Then, to account for the broken free-fall assumptions during collisions, we smooth the estimated velocities with a physically-motivated motion prior. As shown in Figure 2, collisions are much shorter than free-fall periods, indicating that the robot is indeed in free fall during most of the gyroscope saturation period. The following assumptions are made to estimate saturated gyroscope measurements during free fall:

Assumption 1: The IMU is not located along the robot's rotation axis;

Assumption 2: The measured linear acceleration at the robot's COM is null;

Assumption 3: The rotation axis remains unchanged between two IMU measurements;

Assumption 4: The rotation axis passes through the robot's COM;

Assumption 5: Only one axis of the gyroscope is saturated at once.

Assumption 1 is necessary to enable angular velocity estimation from the measured centripetal acceleration. Assumption 2 stems from the fact that the acceleration perceived by a body in free fall is null and on the underlying assumption that the force caused by air friction is negligible. Assumption 3 is supported by the high acquisition rate of IMU measurements, which is typically 100 Hz or more, and by the angular momentum preventing the axis of rotation from changing quickly. Assumption 4 relies on the fact that when no external forces act on a body, it rotates about its COM. This is again based on the underlying assumptions of free-fall conditions and of negligible air friction. Assumption 5 is not strictly necessary, but allows us to compute a simple and precise estimate of the angular speed of a saturated gyroscope axis. Moreover, in our experiments described in Section IV-A, we did not encounter situations in which more than one gyroscope axis was saturated at once.

The important variables are illustrated in Figure 3 where an IMU is linked to the robot's COM by $\boldsymbol{t}$ and rotates at an angular speed $\omega = \|\boldsymbol{\omega}\|$ around the unit rotation axis $\boldsymbol{e}$. The $\boldsymbol{r}$ vector orthogonally links $\boldsymbol{e}$ to the IMU. The rotational coordinate frame $\mathcal{R}$ is at the same location as the IMU, but rotated to have its x axis perpendicular and pointing to the rotation axis $\boldsymbol{e}$ and its z axis in the same direction as $\boldsymbol{e}$. As the axis-angle representation states, the rotation axis $\boldsymbol{e}$ can be recovered from the angular velocity $\boldsymbol{\omega} = [\omega_x, \omega_y, \omega_z]^T$ such that $\boldsymbol{\omega} = \omega \boldsymbol{e}$. Drawing from the work of Pachter *et al.* [11], the Coriolis formula states that

$$\boldsymbol{a}_I = \boldsymbol{a}_C + \dot{\boldsymbol{\omega}} \times \boldsymbol{r} + \boldsymbol{\omega} \times (\boldsymbol{\omega} \times \boldsymbol{r}), \tag{1}$$

where $\boldsymbol{a}_I$ is the linear acceleration at the location of the IMU, $\boldsymbol{a}_C$ is the linear acceleration at the robot's COM, and $\dot{\boldsymbol{\omega}}$ is the angular acceleration of the robot. All angular velocity and linear acceleration measurements are expressed in a common coordinate frame. Since accelerometers measure proper acceleration, the measured acceleration $\tilde{\boldsymbol{a}}_I$ at the location of the IMU is equal to

$$\begin{aligned} \tilde{\boldsymbol{a}}_I &= \boldsymbol{a}_I - \boldsymbol{g} \\ &= (\boldsymbol{a}_C - \boldsymbol{g}) + \dot{\boldsymbol{\omega}} \times \boldsymbol{r} + \boldsymbol{\omega} \times (\boldsymbol{\omega} \times \boldsymbol{r}) \\ &= \tilde{\boldsymbol{a}}_C + \dot{\boldsymbol{\omega}} \times \boldsymbol{r} + \boldsymbol{\omega} \times (\boldsymbol{\omega} \times \boldsymbol{r}), \end{aligned} \tag{2}$$

where $\boldsymbol{g}$ is the gravity force vector and $\tilde{\boldsymbol{a}}_C$ is the measured acceleration at the robot's COM. Using Assumption 2, Equation 2 simplifies to

$$\tilde{\boldsymbol{a}}_I \approx \dot{\boldsymbol{\omega}} \times \boldsymbol{r} + \boldsymbol{\omega} \times (\boldsymbol{\omega} \times \boldsymbol{r}). \tag{3}$$

Equation 3 is the key to allowing the computation of angular velocity during gyroscope saturation periods. The first term

[1] https://github.com/norlab-ulaval/saturated_gryo_speed_estimation

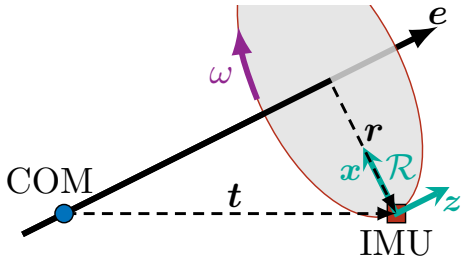

Fig. 3. Illustration of important quantities in our angular velocity estimation method. The COM is indicated by a blue dot. The IMU is indicated by a red square. The axis of rotation $\boldsymbol{e}$ is assumed to pass through the robot's COM. The vector $\boldsymbol{t}$ joins the COM and the IMU and the rotation lever arm $\boldsymbol{r}$ joins the axis of rotation to the IMU. The angular speed ω of the IMU around $\boldsymbol{e}$ is indicated in purple. The x and z axis of the rotational frame $\mathcal{R}$ are illustrated in green.

of the sum is the tangential acceleration of the IMU and is oriented into the page in Figure 3. The second term of the sum is the centripetal acceleration and is oriented in the same direction as the x axis of the rotational coordinate frame $\mathcal{R}$ in Figure 3. Therefore, expressing the accelerometer measurements $\tilde{\boldsymbol{a}}_I$ in the coordinate frame $\mathcal{R}$ and using Equation 3, we can deduce without further approximation that

$$ {}^{\mathcal{R}}\tilde{\boldsymbol{a}}_I \approx \begin{bmatrix} \|\boldsymbol{\omega} \times (\boldsymbol{\omega} \times \boldsymbol{r})\| \\ -\|\dot{\boldsymbol{\omega}} \times \boldsymbol{r}\| \\ 0 \end{bmatrix} = \begin{bmatrix} \omega^2 r \\ -\dot{\omega} r \\ 0 \end{bmatrix}, \tag{4} $$

where $\omega = \|\boldsymbol{\omega}\|$, $r = \|\boldsymbol{r}\|$ and $\dot{\omega} = \|\dot{\boldsymbol{\omega}}\|$. The last equality in Equation 4 holds because $\boldsymbol{r}$ is orthogonal to $\boldsymbol{\omega}$ by definition and to $\dot{\boldsymbol{\omega}}$ due to Assumption 3. The y component of ${}^{\mathcal{R}}\tilde{\boldsymbol{a}}_I$ is negative because the y axis of $\mathcal{R}$ and the IMU tangential acceleration are in opposite directions. From here, the angular velocity can be estimated from either the x or y component of the acceleration vector. However, computing the angular velocity via the angular acceleration $\dot{\boldsymbol{\omega}}$ would lead to integrating noise and thus lead to a less accurate estimate. In order to compute the magnitude of the angular velocity vector $\|\boldsymbol{\omega}\|$, the magnitude of the lever arm $\|\boldsymbol{r}\|$ must be determined. Using Assumption 4, as can be seen in Figure 3, $\boldsymbol{r}$ can be retrieved with

$$ \boldsymbol{r} = \boldsymbol{t} - (\boldsymbol{t} \cdot \boldsymbol{e})\boldsymbol{e}. \tag{5} $$

The axis of rotation $\boldsymbol{e}$ is usually determined using the angular velocity $\boldsymbol{\omega}$, but this is not possible in the present case, since the measurement of one of the gyroscope axes is saturated. Using Assumption 3, the axis of rotation of the previous estimated angular velocity is used instead. Lastly, without loss of generality, let us assume that the gyroscope is saturated on the x component. Using Assumption 1 and Assumption 5, we can retrieve the saturated measurement ω_x using

$$ \omega_x = \sqrt{\frac{\tilde{a}_x}{\|\boldsymbol{t} - (\boldsymbol{t} \cdot \boldsymbol{e})\boldsymbol{e}\|} - \omega_y^2 - \omega_z^2}, \tag{6} $$

where $\tilde{a}_x$ is the x component of ${}^{\mathcal{R}}\tilde{\boldsymbol{a}}_I$, ω_y and ω_z are the unsaturated gyroscope measurements. Due to the noise in accelerometer measurements, the computed angular speed might be below the saturation point, which is not possible. To solve this, we conserve the maximum between the estimated angular speed magnitude and the saturation point. The sign ambiguity of the computed angular speed can be resolved by considering the sign of the saturated gyroscope measurement. Again, due to the noise in accelerometer measurements, the term under the radical in Equation 6 can be negative. In that case, we simply reject the estimate. We are left with Equation 6 to estimate the angular velocity when a saturation is detected using a threshold on gyroscope measurements.

We now smooth the angular velocity estimates computed previously with Gaussian Processes (GPs) using a physically-motivated motion prior. GPs allow us to obtain more accurate angular velocity estimates during collisions, when our free-fall assumptions are broken. Similarly to what was done by Tang *et al.* [21], a white-noise-on-jerk motion prior is used. To account for the possibly abrupt changes in angular velocity, the diagonal entries of the angular jerk power spectral density matrix are set to a high value $q_{\ddot{\omega}}$. The unsaturated gyroscope measurements are assigned a covariance of $\sigma_{\tilde{\omega}}^2$, which is computed using the IMU specifications. The valid angular speed estimates are given a higher covariance, $\sigma_{\hat{\omega}}^2$, which is a parameter of our method. Employing GPs for smoothing has the advantage of yielding both the mean and covariance of the estimated angular velocity as functions of time. The STEAM library, from Anderson *et al.* [22], was used to carry out these computations.

B. SLAM framework

The SLAM framework in which our angular velocity estimation method is inserted is divided into four steps which are described briefly in this section. For more details, refer to our previous work [5]. **1) Intra-scan trajectory estimation:** Using the estimated angular velocities and accelerometer measurements, the trajectory of the IMU is estimated. To do so, first, the angular velocities and linear accelerations are passed through a Madgwick filter [23] to estimate the orientation of the IMU throughout the scan. These orientations are used to remove the gravity vector from accelerometer measurements. Then, accelerometer measurements are integrated, and resulting displacements are added to the position computed in the previous registration to estimate the position of the IMU throughout the scan. Finally, this position and orientation information is used in combination with the extrinsic calibration between the IMU and lidar to compute the trajectory of the latter during the scan. **2) Deskewing:** As lidar sensors typically assume they are static during scans [5], point positions need to be corrected with respect to intra-scan motion. The poses of the lidar previously estimated at each IMU measurement time are linearly interpolated to transform every measured point in the coordinate frame of the lidar at the beginning of the scan. **3) Uncertainty-aware registration:** Using the Time-based Weighting (TW) model and registration algorithm described in [5], the deskewed scans are registered to the reconstructed map of the environment. This weighting model takes the uncertainty of the deskewing into account for the registration algorithm by assigning a larger weight to scan

points that are likely to be less affected by skewing. As the estimated displacement of the lidar during the scan is used as a prior alignment for the registration algorithm, the quality of IMU measurements has a major influence on the robustness of registration. **4) Merge and map maintenance:** The registered deskewed scan is then merged into the map of the environment and maintenance operations are performed. These maintenance operations are surface normal computation and removal of points with a deskewing uncertainty above σ_p^2.

IV. RESULTS

In this section, we describe the experimental setup used to build our dataset. We show that our angular speed estimation method significantly reduces the angular velocity error in the case of gyroscope-saturating motions. We then show the robustness improvement for our SLAM framework, both for localization and mapping. Lastly, we compare the range of motions in our dataset to those in other SLAM datasets.

A. Experimental setup

To validate the improvements reached through our approach while minimizing hardware damage and replacement costs, we created a rugged perception rig, which is shown in Figure 1. A RoboSense RS-16 lidar was used to record the 3D point clouds at a frequency of $10\,\mathrm{Hz}$. For angular velocity measurements, we used two different IMUs, with distinct gyroscope saturation points. The first IMU is an XSens MTi-30, with a gyroscope saturating at $10.5\,\mathrm{rad/s}$, despite the Xsens specification sheet stating a saturation point of $7.85\,\mathrm{rad/s}$. The second IMU is a VectorNav VN-100, with a gyroscope saturating at $34.9\,\mathrm{rad/s}$ according to its specification sheet. Its angular velocity measurements are used as ground truth since we did not reach its gyroscope saturation point in our dataset. Lastly, we used a Raspberry Pi 4 embedded computer to record all sensor data. All SLAM results were computed offline, using the `norlab_icp_mapper` library [24]. The COM of the rig was evaluated manually, by balancing the rig on a single point on each face. The constants that were introduced in Section III are set to $q_{\ddot{\omega}} = 10^6$, $\sigma_{\ddot{\omega}}^2 = 2.74 \times 10^{-5}$, $\sigma_{\hat{\omega}}^2 = 3.65$ and $\sigma_p^2 = 1$. The value of $\sigma_{\hat{\omega}}^2$ was computed from the MTi-30 datasheet and the values of $q_{\ddot{\omega}}$ and σ_p^2 are hyperparameters of our method. To evaluate our method, we built the TIGS dataset, including a total of 32 distinct runs, consisting of pushing the rig to roll down a steep hill, mimicking a tumbling robot. One of the runs of our dataset can be seen in Figure 1. A ground-truth map was built by moving the sensor rig slowly, thus limiting skew in the scans.

B. Angular velocity estimation

Using the angular velocity estimation method described in Section III-A, the angular velocity of the platform was estimated for all of the runs in our dataset. An example is shown for a single run in the left subplot of Figure 4. Our method was applied to the MTi-30 measurements and the VN-100 measurements were used as ground truth. The speed estimation error during gyroscope saturation periods with and without our method is shown for all runs in our dataset in the right part of Figure 4. Only periods of saturation are studied (i.e., the light gray area), as angular velocities are the same with or without our speed estimation method outside the saturation zones. When accounting for all runs, our approach reduces the angular velocity error median by $83.4\,\%$, when compared to saturated gyroscope measurements. As expected, our angular velocity estimation approach significantly reduces the angular velocity error under gyroscope saturations, especially for extreme values. The spikes in estimated angular velocity are due to the free-fall assumptions which are no longer valid at the moment of collisions.

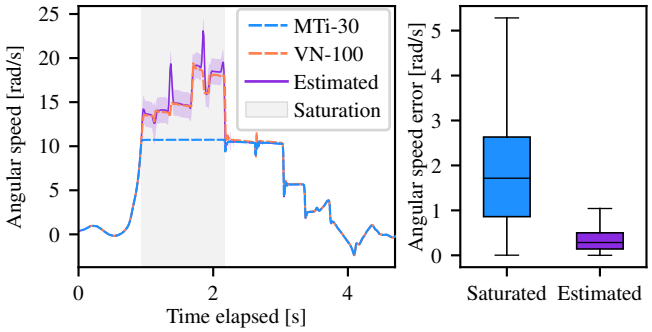

Fig. 4. The left plot shows an example of the angular speed through time for the saturated gyroscope axis for a single run of our experiments. The measurements from an MTi-30 gyroscope are shown in dashed blue, the measurements from a VN-100 gyroscope are indicated in dashed orange, and the angular speeds estimated with our method using MTi-30 measurements are illustrated in purple. The purple-shaded area represents three standard deviations above and below the estimated speed. The right plot shows the error in angular speed without (in blue) and with (in purple) our method during saturation periods for all runs.

C. Impact on SLAM

Using no prior map of the environment, our SLAM algorithm described in Section III-B was run on each of the 32 runs in our dataset. The localization errors with and without our angular velocity estimation method are illustrated in Figure 5. Here, the localization error corresponds to the error in the estimated transformation between the initial and final poses of the rig. The ground-truth transformation for each run was found by registering the first and last scan in the ground-truth map, as the perception rig is static at these times. Our angular velocity estimation approach improves the baseline SLAM algorithm localization error median by $71.5\,\%$ for translation and $65.5\,\%$ for rotation.

To investigate the impact of our method on mapping, we analyze a map built with our SLAM system for every run in our dataset. We built on prior work from Chung *et al.* [25] for the Defense Advanced Research Projects Agency (DARPA) Subterranean Challenge to evaluate mapping quality. Our map overlap metric is the percentage of reconstructed map points that are within a threshold distance from a point belonging to the ground-truth map. In the present case, we chose the threshold distance to be $0.25\,\mathrm{m}$ as opposed to the $1\,\mathrm{m}$ from the work of Chung *et al.* [25] to reflect the much smaller scale of our experiments. Indeed, the distance traveled in our runs is between $5\,\mathrm{m}$ and $10\,\mathrm{m}$, compared

to between $150\,\mathrm{m}$ and $250\,\mathrm{m}$ in the case of the DARPA Challenge. The mean overlap of the maps built without our angular velocity estimation method is $77.2\,\%$, as opposed to $92.1\,\%$ with our method. The result for a specific run is shown in Figure 6. We selected this run since the increase in mapping performance was significant when our SLAM algorithm relied on our speed estimation method. Additionally, we define mapping failures as cases where the percentage of outliers in the reconstructed map (i.e., points farther than $0.25\,\mathrm{m}$ from their closest neighbor in the ground-truth map) is above $15\,\%$. With saturated gyroscope measurements, we observe a failure of the mapping for 12 out of the 32 runs, as opposed to no failure when relying on our speed estimation method. This clearly shows that our angular velocity estimation method increases mapping robustness in the case of a robot tumbling down a hill.

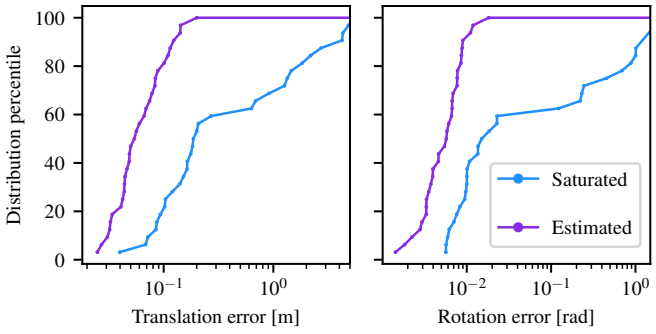

Fig. 5. Localization error for every run in the dataset. The percentiles of translation error distribution is shown on the left plot and the percentiles of rotation error distribution is shown in the right plot. The blue and purple lines represent the percentiles of the localization error distribution when relying on saturated measurements and our speed estimation method, respectively. Errors on both subplots are shown with a log scale.

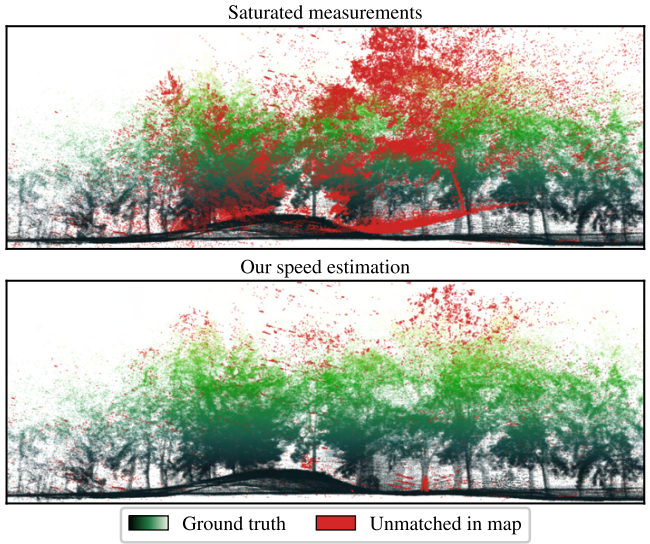

Fig. 6. Side view of the ground-truth map built for the dataset. The color map is proportional to the point height. Mapping outliers from the fourteenth run are displayed in red. The top map shows the mapping outliers when relying on saturated measurements. The bottom map shows the mapping outliers when using our speed estimation method. Outlier points are defined as points that are farther than $0.25\,\mathrm{m}$ from the ground-truth map.

D. The TIGS Dataset

To show how our Tumbling-Induced Gyroscope Saturation (TIGS) dataset covers a larger spectrum of aggressive motions than other mechanical lidar SLAM datasets, we present the distributions for observed linear accelerations and angular velocities in Figure 7, in comparison to the KITTI [20], Newer College [18] and Hilti-Oxford [19] datasets. One can observe that our dataset covers a significantly larger spectrum of aggressive motions, characterized by high linear accelerations and angular velocities. Indeed, the maximum recorded linear acceleration for the TIGS dataset is $127.1\,\mathrm{m/s^2}$ over the highest linear acceleration observed in the compared datasets. Since the saturation point of the VN-100 accelerometer was reached for some collisions, the increase in linear acceleration that was actually sustained is probably higher than this number. Furthermore, the maximum angular speed for the TIGS dataset is $13.9\,\mathrm{rad/s}$ over the highest angular speed observed in the compared datasets. Our dataset is the only one with angular speeds over the specified saturation point of the Xsens gyroscope, thus allowing us to evaluate SLAM pipelines under saturated gyroscope measurements.

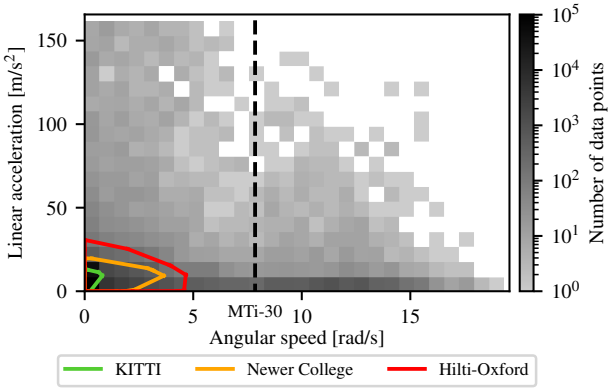

Fig. 7. Density map of the TIGS dataset. The grayscale represents the number of data points acquired at the specific angular speeds and linear accelerations. The outlines represent the distributions in linear accelerations and angular velocities for similar datasets. The KITTI dataset is shown in green, the Newer College dataset is indicated in orange, and the Hilti-Oxford dataset is illustrated in red. The dashed line represents the manufacturer-specified saturation point of the MTi-30 gyroscope.

V. CONCLUSION

In this paper, we introduced a novel method to estimate angular speed under saturated gyroscope measurements. We validated our method through 32 runs mimicking a robot tumbling down a hill, with angular speeds reaching up to $18.6\,\mathrm{rad/s}$ and linear accelerations up to $157.8\,\mathrm{m/s^2}$. Our system was able to perform SLAM under these aggressive motions with no mapping failure, while it failed on $37.5\,\%$ of the runs without our speed estimation method. We release our dataset, called TIGS, to allow evaluation of SLAM frameworks under aggressive motions. Future work involves quantifying the error of our method through a complete trajectory with a motion capture system and performing a thorough comparison with Point-LIO [14].

References

[1] K. Nagatani, S. Kiribayashi, Y. Okada, K. Otake, K. Yoshida, S. Tadokoro, T. Nishimura, T. Yoshida, E. Koyanagi, M. Fukushima, and S. Kawatsuma, "Emergency response to the nuclear accident at the Fukushima Daiichi Nuclear Power Plants using mobile rescue robots," *Journal of Field Robotics (JFR)*, vol. 30, no. 1, pp. 44–63, 2013.

[2] L. Dilaveroglu and O. Ozcan, "MiniCoRe: A Miniature, Foldable, Collision Resilient Quadcopter," in *3rd IEEE International Conference on Soft Robotics (RoboSoft)*, 2020.

[3] K. Ebadi, L. Bernreiter, H. Biggie, G. Catt, Y. Chang, A. Chatterjee, C. E. Denniston, S.-P. Deschênes, K. Harlow, S. Khattak, L. Nogueira, M. Palieri, P. Petráček, M. Petrlík, A. Reinke, V. Krátký, S. Zhao, A.-A. Agha-Mohammadi, K. Alexis, C. Heckman, K. Khosoussi, N. Kottege, B. Morrell, M. Hutter, F. Pauling, F. Pomerleau, M. Saska, S. Scherer, R. Siegwart, J. L. Williams, and L. Carlone, "Present and Future of SLAM in Extreme Environments: The DARPA SubT Challenge," *IEEE Transactions on Robotics (T-RO)*, Oct. 2023.

[4] G. Williams, P. Drews, B. Goldfain, J. M. Rehg, and E. A. Theodorou, "Information-Theoretic Model Predictive Control: Theory and Applications to Autonomous Driving," *IEEE Transactions on Robotics (T-RO)*, vol. 34, no. 6, pp. 1603–1622, Dec. 2018.

[5] S.-P. Deschênes, D. Baril, V. Kubelka, P. Giguère, and F. Pomerleau, "Lidar Scan Registration Robust to Extreme Motions," in *2021 18th Conference on Robots and Vision (CRV)*, IEEE, 2021, pp. 17–24.

[6] J. Lee, H. Kim, S. H. Oh, J. C. Do, C. W. Nam, D. H. Hwang, and S. J. Lee, "Angular velocity estimation of rotating plate using extended Kalman filter with accelerometer bias model," *Microsystem Technologies*, vol. 25, pp. 2855–2867, 7 Jul. 2019.

[7] T. Shan, B. Englot, D. Meyers, W. Wang, C. Ratti, and D. Rus, "LIO-SAM: Tightly-coupled lidar inertial odometry via smoothing and mapping," in *2020 IEEE/RSJ International Conference on Intelligent Robots and Systems (IROS)*, pp. 5135–5142.

[8] A. Reinke, M. Palieri, B. Morrell, Y. Chang, K. Ebadi, L. Carlone, and A. A. Agha-Mohammadi, "LOCUS 2.0: Robust and Computationally Efficient Lidar Odometry for Real-Time 3D Mapping," *IEEE Robotics and Automation Letters (RA-L)*, vol. 7, pp. 9043–9050, 4 Oct. 2022.

[9] W. Xu, Y. Cai, D. He, J. Lin, and F. Zhang, "FAST-LIO2: Fast Direct LiDAR-Inertial Odometry," *IEEE Transactions on Robotics (T-RO)*, vol. 38, pp. 2053–2073, 4 Aug. 2022.

[10] K. Chen, R. Nemiroff, and B. T. Lopez, "Direct LiDAR-Inertial Odometry: Lightweight LIO with Continuous-Time Motion Correction," in *2023 IEEE International Conference on Robotics and Automation (ICRA)*, pp. 3983–3989.

[11] M. Pachter, T. C. Welker, and R. E. Huffman, "Gyro-free INS Theory," *NAVIGATION*, vol. 60, no. 2, pp. 85–96, 2013.

[12] A. Segal, D. Haehnel, and S. Thrun, "Generalized-ICP," in *Robotics: Science and Systems (RSS) V*, Robotics: Science and Systems Foundation, 2009.

[13] M. Palieri, B. Morrell, A. Thakur, K. Ebadi, J. Nash, A. Chatterjee, C. Kanellakis, L. Carlone, C. Guaragnella, and A.-a. Agha-mohammadi, "LOCUS: A Multi-Sensor Lidar-Centric Solution for High-Precision Odometry and 3D Mapping in Real-Time," *IEEE Robotics and Automation Letters (RA-L)*, vol. 6, no. 2, pp. 421–428, 2021.

[14] D. He, W. Xu, N. Chen, F. Kong, C. Yuan, and F. Zhang, "Point-LIO: Robust High-Bandwidth Light Detection and Ranging Inertial Odometry," *Advanced Intelligent Systems*, vol. 5, 7 Jul. 2023.

[15] Q. Dang and Y. Suh, "Sensor Saturation Compensated Smoothing Algorithm for Inertial Sensor Based Motion Tracking," *Sensors*, vol. 14, pp. 8167–8188, 5 May 2014.

[16] C. H. Tan, D. S. bin Shaiful, E. Tang, J.-Y. Khaw, G. S. Soh, and S. Foong, "Flydar: Magnetometer-based High Angular Rate Estimation during Gyro Saturation for SLAM," in *2020 IEEE International Conference on Robotics and Automation (ICRA)*, pp. 8532–8537.

[17] M. Silic and K. Mohseni, "Correcting Current-Induced Magnetometer Errors on UAVs: An Online Model-Based Approach," *IEEE Sensors Journal*, vol. 20, pp. 1067–1076, 2 Jan. 2020.

[18] M. Ramezani, Y. Wang, M. Camurri, D. Wisth, M. Mattamala, and M. Fallon, "The Newer College Dataset: Handheld LiDAR, Inertial and Vision with Ground Truth," in *2020 IEEE/RSJ International Conference on Intelligent Robots and Systems (IROS)*, pp. 4353–4360.

[19] L. Zhang, M. Helmberger, L. F. T. Fu, D. Wisth, M. Camurri, D. Scaramuzza, and M. Fallon, "Hilti-Oxford Dataset: A Millimeter-Accurate Benchmark for Simultaneous Localization and Mapping," *IEEE Robotics and Automation Letters (RA-L)*, vol. 8, pp. 408–415, 1 Jan. 2023.

[20] A. Geiger, P. Lenz, and R. Urtasun, "Are we ready for autonomous driving? The KITTI vision benchmark suite," in *2012 IEEE Conference on Computer Vision and Pattern Recognition*, pp. 3354–3361.

[21] T. Y. Tang, D. J. Yoon, and T. D. Barfoot, "A White-Noise-on-Jerk Motion Prior for Continuous-Time Trajectory Estimation on SE(3)," *IEEE Robotics and Automation Letters*, vol. 4, no. 2, pp. 594–601, 2019.

[22] S. Anderson and T. D. Barfoot, "Full STEAM ahead: Exactly sparse gaussian process regression for batch continuous-time trajectory estimation on SE(3)," in *2015 IEEE/RSJ International Conference on Intelligent Robots and Systems (IROS)*, pp. 157–164.

[23] S. O. H. Madgwick, A. J. L. Harrison, and R. Vaidyanathan, "Estimation of IMU and MARG orientation using a gradient descent algorithm," in *2011 IEEE International Conference on Rehabilitation Robotics*, pp. 1–7.

[24] D. Baril, S.-P. Deschênes, O. Gamache, M. Vaidis, D. LaRocque, J. Laconte, V. Kubelka, P. Giguère, and F. Pomerleau, "Kilometer-scale autonomous navigation in subarctic forests: challenges and lessons learned," *Field Robotics*, vol. 2, no. 1, pp. 1628–1660, Mar. 2022.

[25] T. H. Chung, V. Orekhov, and A. Maio, "Into the Robotic Depths: Analysis and Insights from the DARPA Subterranean Challenge," *Annual Review of Control, Robotics, and Autonomous Systems*, vol. 6, no. 1, pp. 477–502, 2023.